Nanocrystal Superlattice Imaging by Atomic Force Microscopy

Peter K. Stoimenov[1], Savka I. Stoeva[1], B. L. V. Prasad[1], Christopher M. Sorensen[2], Kenneth J. Klabunde[1]
Department of Chemistry[1] and Department of Physics[2], Kansas State University, Manhattan, Kansas 66506

ABSTRACT

Applicability of Atomic Force Microscopy (AFM) for structural characterization of nanocrystal superlattices is demonstrated on high-resolution imaging of superlattices formed by thiol stabilized gold nanoparticles on carbon coated and hydrophobic supports. Thin (<1nm) uniform coating of the samples with metal film before imaging was found to eliminate the undesirable effects of tip-sample interaction. Size and interparticle spacing are in excellent agreement with transmission electron microscopy results. AFM can be used as a complementary technique for nanocrystal superlattice structural characterization providing possibilities for crystal growth investigation on a variety of supports of practical interest and high resolution of the surface structure of superlattice structures .

1. INTRODUCTION

Preparation of long-range ordered nanoparticle assemblies, known as nanocrystal superlattices (NCSs), is a blossoming field of research[1]. The attention given to these new materials comes from fundamental chemical and physical interest, as well as from the large variety of applications where nanocrystal superlattices could be used as part of optical and electronic devices, sensing units, bioprobes, and catalysts[1].

The most widely used techniques for nanocrystal superlattice structural characterization are transmission electron microscopy (TEM) and X-ray diffraction (XRD) [1, 2]. There are, however, some constraints imposed by these techniques. A limited number of supports can be used for TEM imaging and sometimes the nanocrystal superlattice can change under the influence of the electron beam. TEM can be used to probe the superlattices only at places where the amount of deposited material is not too thick for the electron beam to penetrate. XRD provides information averaged over the whole sample, but can not provide local structural information. One major question that TEM and XRD can not answer is whether the long-range order in a superlattice is preserved on its surface as it exists in the bulk. No information about the state of the ligand shell on the nanoparticles' surface can be provided as well.

Understanding the surface structure of a nanocrystal superlattice is important since many factors such as surface tension and interaction with the surrounding liquid during the drying process influence the surface of the generated solid phase and could lead to surface reconstruction or to a lack of ordering on the surface despite ordering in the bulk phase superlattice.

Despite the fact that AFM has been used for imaging of a variety of surfaces with features on the same dimensions as nanoparticle superlattices, such as lithography patterned surfaces[3, 4], crystal growth of viruses[5] and polymer particles[6], there are not specific examples of resolving separate particles in nanocrystal superlattice structures by AFM. AFM studies of metal colloidal solutions deposited on a support deal with isolated nanoparticles or aggregates of particles[7]. AFM is used for site-selective positioning of nanoparticles as aggregates or as thin films on a substrate[8].

Herein, we present a simple, yet efficient way, to image nanocrystal superlattices by AFM. It is exemplified by AFM characterization of nanocrystal superlattices formed by gold nanoparticles stabilized by alkanethiols.

Physical Chemistry of Interfaces and Nanomaterials III, edited by Gregory V. Hartland, Xiao-Yang Zhu, Proceedings of SPIE Vol. 5513 (SPIE, Bellingham, WA, 2004)
0277-786X/04/$15 · doi: 10.1117/12.558429

2. EXPERIMENTAL SECTION

2.1 Materials. All chemicals were used as received without further purification. (3-mercaptopropyl)trimethoxysilane ($HS(CH_2)_3Si(OCH_3)_3$, 95%) was obtained from Aldrich. All other reagents were purchased from Fisher. Toluene was dried over a molecular sieve. Ultrahigh purity water (18.2 MΩ, Millipore) was used throughout the experiments.

2.2 Gold Colloid Preparation. Decanethiol and dodecanethiol stabilized gold nanoparticles with an average diameter of 4.7 nm (as determined by TEM) were prepared by a procedure described in details in Ref. 10. Shortly, the procedure consists of reduction of $AuCl_3$ dissolved in toluene by aqueous $NaBH_4$ in the presence of didodecyldimethylamonium bromide. This method produces high quality gold nanoparticles with a strong tendency towards superlattice formation.

2.2 Hydrophobic Substrate Preparation. Glass slides (15 mm diameter, Ted Pella, Inc.) were rigorously washed with piranha solution (1:4 H_2O_2/conc. H_2SO_4) for 2h. The slides were thoroughly washed with water and dried at 110°C. The slides were submerged in 10 wt% (3-mercaptopropyl)trimethoxysilane in anhydrous toluene for 20 min, washed with methanol and dried.

2.3 Carbon Coated Substrate Preparation. Thin carbon film was evaporated under vacuum onto pre-cleaned glass slides as described above using a Kinney KDTG-3P carbon sputter.
Sample preparation. 10μl of gold nanoparticle solution in toluene was deposited on a substrate and left undisturbed for 2-3 weeks covered with a Petri dish to ensure slow evaporation of the solvent leading to large nanocrystal superlattice formation. Samples were uniformly coated under vacuum with a very thin metal layer (< 1nm, Au/Pd alloy) using a Denton sputter coater.

2.4 AFM Imaging. Sample imaging was performed on a Nanoscope IIIa (Digital Instruments) in tapping mode using Olympus OTESPA 125 μm tips with typical resonance frequency of 300 kHz. Typical scan parameters were: scan angle 0°, scan rate 0.2-0.5 Hz. Special care was taken to decrease the humidity level in the AFM chamber.

3. RESULTS AND DISCUSSION

3.1 The resolution of ordered superlattice structures is strongly limited by the presence of stabilizing ligands (most often alkanethiols, alkaneamines, etc.) on the surface of the particles that interact with the scanning probe tip. In general, the superlattices are prepared in the presence of excess stabilizing ligand. This excess of ligand is captured in the superlattice structure. Since most widely used ligands such as amines and thiols are liquids at ambient conditions, the imaging by AFM is practically impossible since the capillary forces between an AFM tip and the liquid present in the material can be several orders of magnitude stronger than those of the tip-sample surface interaction. On the other hand, removal of the excess ligand is undesirable as it causes 'stripping' of the particles and change in the interparticle distance[10]. Other potential factors for the lack of surface structure resolution is particle displacement from the support and damaging of the soft superlattice surfaces by the AFM tip (especially in the contact mode of operation).

Our previous TEM results demonstrate that decanethiol and dodecanethiol stabilized gold nanoparticles investigated by AFM in the present paper, organize into long-range ordered nanocrystal superlattices when deposited on carbon-coated TEM grids[9, 11]. Nanocrystal superlattices imaged by TEM are found to have a variety of shapes (Figure 1).

The focus of the AFM studies here are both $C_{10}H_{21}SH$- and $C_{12}H_{25}SH$- protected gold nanoparticles aiming to emphasize the versatility of the approach. Superlattices built of $C_{10}H_{21}SH$- functionalized particles melt at lower temperature compared to the $C_{12}H_{25}SH$-functionalized system and thus they are easily susceptible to melting by the electron beam.

In this study we used two types of support- carbon and thiol derivatized glass. Carbon coated glass is used to mimic the carbon coated TEM grid surface, where superlattice formation occurs easily. The thiol derivatized surface has a strong affinity to bind gold nanoparticles. In our experiments we did not observe significant differences in the properties of the superlattices grown on one or the other support. Thus, we believe, AFM could be used for investigation of superlattice structures grown on any modified surface.

3.2 AFM of nanocrystal superlattices stabilized by $C_{10}H_{21}SH$ on hydrophobic glass supports.

Large area TM(tapping mode)-AFM scans of nanocrystal superlattices formed by $C_{10}H_{21}SH$- stabilized Au nanoparticles on hydrophobic glass supports confirm that the gold nanoparticles organize in large arrays (Figure 2). Evenly distributed superlattice structures with lateral dimensions of 3 to 10 μm are visible from the images. A magnified AFM image shows the presence of structures that tend to have regular shapes (e.g. pentagonal island in Figure 2b). Our previous TEM studies showed the abundant presence of well faceted and regularly shaped structures [12]. A cross-section of the superlattice structures (Figure 2c) showed that their height varies between 400 and 450 nm. Such information can not be obtained by TEM since it gives only a two-dimensional projection of the image. The dimensions of the superlattice islands are possible indications that the superlattice growth occurred on the interface between the support and the solution. Homogenous nucleation and growth in solution are not likely since the weight of the superlattice is rather large, so that it would be difficult to remain in the liquid phase.

Another interesting feature visible for the AFM images (Figure 2) is that all superlattice structures are surrounded by scattered material designated by arrows in Figure 2a. This scattered material is made up of excess thiol and separate Au nanoparticles surrounding the superlattice structures as observed by TEM (Figure 1d). The reason for this phenomenon is likely due to lateral capillary forces during the process of superlattice formation. Similar effects were found in cases of crystal growth of proteins, viruses and latex particles[13].

Figure 3 illustrates the resolved edge structure of one of the superlattices presented in Figure 2. Noteworthy is the high resolution of the structured edges, where a 'terrace' arrangement of the particles is clearly visible. The cross-section (Figure 3) has repetitive steps with heights between 15.4 and 17 nm. The width of each step is around 5.6 nm which infers that each step is composed of one particle in width (taken into account that the AFM 'feels' the decanethiol molecules adsorbed on the particle surface). Resolved steps infer that layering of the particles occurs in order, thus keeping the arrangement three dimensional rather than a disordered pile of nanoparticles.

3.3 AFM of nanocrystal superlattices stabilized by $C_{12}H_{25}SH$ on hydrophobic glass supports.

A well resolved TM-AFM image of the surface of a nanocrystal superlattice formed by $C_{12}H_{25}SH$- functionalized Au nanoparticles was obtained on a carbon coated support (Figure 4a). The cross-section (Figure 4d) gives a most frequently measured center to center interparticle spacing of 5.6 nm and the cross-section in Figure 4e presents a most frequently measured center to center interparticle spacing of 8.2 nm. Such values were reproducibly measured across the whole sample. The data obtained by AFM for interparticle spacing support that the scanned surface in Figure 4a is the $(100)_{SL}$ surface of face-centered cubic (*fcc*) superlattice (the subscript SL designates planes and directions in the nanocrystal superlattice). The results are in excellent agreement with the earlier TEM data which showed that the gold particles are ordered in an *fcc* superlattice (confirmed by electron diffraction[12]) with a most frequently measured lattice constant of 8.9 nm[12]. AFM images confirmed that the ordering in the bulk superlattice is indeed preserved on its surface. Similar results were obtained in the case of superlattice growth on thiol-derivatized glass substrate. Representative TM-AFM images of NCS composed of $C_{12}H_{25}SH$- functionalized Au nanoparticles on hydrophobic supports are shown in Figure 5. AFM results demonstrate that the *fcc* type of ordering is preserved and the interparticle spacings are the same as in the case of samples deposited on carbon coated supports. The drift experienced in imaging (Figures 4 and 5) we attribute to the weak Van der Waals interaction between the nanoparticles. It is reasonable to believe that such change of position of nanoparticles can be easily induced by the tip as the particles are being held in place only by very weak interactions with their neighbors.

The cross section along the [110] direction of the *fcc* superlattice (Figure 4d) gives the diameter of an individual nanoparticle to be around 5.6 nm. Such a number is in an excellent agreement with the size measured by TEM (4.7 nm) considering that AFM tip also 'feels' the dodecanethiol molecules on the particle surface (~1.6 nm chain length). Taking into account the diameter of the particles and the interparticle spacing, it is reasonable to expect that there is a complete interdigitation of the dodecanethiol molecules along the [110] direction of the *fcc* lattice (see schematic representation in Figure 4e). Therefore the gold particles are tightly arranged along the [110] direction. The tight assembly in this case leads to the absence of any widening effect of the lateral size of the nanoparticles imaged by AFM due to the absence of convolution of the finite tip apex size with the sample[14]. A reasonable explanation for this is the fact that the tip does not describe the particles lying alone on a surface, but rather tightly ordered next to each other.

Thus, the tip maps only the top part of the particles avoiding the main cause of the artificial enlargement, namely tapping on the sides of the particles. Reduction of the convolution effect was also observed in the case of colloidal particles arranged in smectic layers[15].

However, gold nanoparticle diameters turn out to be artificially enlarged if measured from the cross section (Figure 4e) (values in the range 7.9 to 8.2 nm are obtained). In this direction the particles are not tightly arranged and the convolution effect of the tip-sample interaction is apparent. The interparticle spacing (8.2 nm), which as discussed above is in a good agreement with the TEM results, infers that in this direction there is no interpenetration of the stabilizing thiol molecules (as shown schematically in Figure 4f). As a result the AFM tip can partially penetrate in the gap between the particles resulting in artificial broadening of the particle diameter due to the convolution of the finite tip size and the sample features.

5. CONCLUSIONS

In summary, the applicability of AFM is demonstrated for structural characterization of nanocrystal superlattices composed of gold nanoparticles stabilized by decanethiol and dodecanethiol ligands. Uniform thin coatings of the samples allowed high resolution of the superlattice structures by eliminating problems such as the predictable presence of excess ligand. Size and interparticle spacing determined by AFM were found to be in excellent agreement with TEM results. To our knowledge these are the first results with AFM, which resolve a long-range ordered nanocrystal superlattice composed of nanoparticles with such small sizes (~5 nm). This study is important because it shows that AFM can be used as a complementary technique for nanocrystal superlattice characterization providing important information about size, shape, thickness of superlattices, as well surface structure resolution and possibility for use practically any support for nanocrystal growth.

We have used the AFM experiment to determine the configuration of nanoparticles on a flat plane of the surface. The AFM experiment allowed the observation of both the nanoparticles 'core' and the shell of ligands which can not be observed by other conventionally techniques. It allowed developing a hypothesis of the ligands interpenetration in the nearest neighbor direction.

The described experiment could be used as a model to study similar materials which can not be imaged successfully by TEM such as samples containing excessive amount organic material or one which forms relatively thick layers.

Acknowledgement. The support of the National Aeronautics and Space Administration (NASA) and partial NSF support for the AFM (DMR-0076169) are acknowledged with gratitude.

Supporting Information. Low magnification TEM micrograph of nanocrystal superlattices composed of gold nanoparticles.

REFERENCES

1. a) Murray, C. B.; Kagan, C. R.; Bawendi, M. G. *Annu. Rev. Mater. Sci.*, **30**, 545-610, 2000.
b) Collier, C. P.; Vossmeyer, T.; Heath, J. R. *Annu. Rev. Phys. Chem.*, **49**, 371-404, 1998.
c) Stoeva, S.; Klabunde, K. J.; Sorensen, C. M.; Dragieva, I. *J. Am. Chem. Soc.*, **124**, 2305-2311, 2002.
d) Lin, X. M.; Jaeger, H.M.; Sorensen, C. M.; Klabunde, K. J. *J. Phys. Chem. B*, **105**, 3353-3357, 2001.
e) Klein, D. L.; Roth, R.; Lim, A. K.; Alivisatos, A. P.; McEuen, P. L. *Nature*, **389**, 1-2, 1997.
f) Harfenist, S. A.; Wang, Z. L.; Whetten, R. L.; Vezmar, I.; Alvarez, M. M. *Adv. Mat.*, **9**, 817-822, 1997.

2. a) Wang, Z. L. *Adv. Mat.*, **10**, 13-30, 1998.
b) Wang, Z. L.; Dai, Z.; Sun, S. *Adv. Mat.*, **12**, 1944-1946, 2000.
c) Connolly, S.; Fullam, S.; Korgel, B.; Fitzmaurice, D. *J. Am. Chem. Soc.*, **120**, 2969-2970, 1998.
d) Sun, S.; Murray, C. B.; Weller, D.; Folks, L.; Moser, A. *Science*, **287**, 1989-1992, 2000.

e) Whetten, R. L.; Shafigullin, M. N.; Khoury, J. T.; Schaaff, T. G.; Vezmar, I.; Alvarez, M. M.; Wilkinson, A. *Acc. Chem. Res.*, **32**, 397-406, 1999.

3. Hansma, P. K.; Elings, V. B.; Marti, O.; Bracker, C. E. *Science*, **242**, 209-242, 1988.

4. a) Hong, S.; Mirkin, C. A. *Science*, **288**, 1808, 2000.
b) Ivanisevic, A.; Mirkin, C. A. *J. Am. Chem. Soc.*, **123**, 7887-7889, 2001.
c) Su, M.; Liu, X.; Li, S.; Dravid, V. P.; Mirkin, C. A. *J. Am. Chem. Soc.*, ASAP, 2003.
d) Lee, K.; Lim, J.; Mirkin, C. A. *J. Am. Chem. Soc.*, ASAP, 2003.
e) Malinsky, M. D.; Kelly, K. L.; Schatz, G. C.; Van Duyne, R. P. *J. Am. Chem. Soc.*, **123**, 1471-1482, 2001.
f) Haynes, C. L.; Van Duyne, R. P. *J. Phys. Chem. B.*, **105**, 5599-5611, 2001.
g) Frey, W.; Woods, C. K.; Chilkoti, A. *Adv. Mat.*, **12**, 1515-1519, 2000.
h) Kitajima, T.; Liu, B.; Leone, S. R. *Appl. Phys. Lett.*, **80**, 497-499, 2002.

5. a) Malkin, A. J.; Kuznetsov, Y. G.; Lucas, R. W.; McPherson, A. *J. Str. Biol.*, **127**, 35-43, 1999.
b) Maeda, H. *Langmuir*, **13**, 4150-4161, 1997.
c) Malkin, A. J.; Land, T. A.; Kuznetsov, Y. G.; McPherson, A.; DeYoreo, J. J. *Phys. Rev. Lett.*, **75**, 2778-2781, 1995.

6. a) Hoog, E.; Steensel, L.; Shel, M.; Eerden, J.; Lekkerkerker, H. *Langmuir*, **17**, 5486-5490, 2001.
b) Dokou, E.; Barteau, M. A.; Wagner, N. J.; Lenhoff, A. M. *J. Coll. Interface Sci.*, **240**, 9-16, 2001.

7. a) Kooij, E. S.; Brouwer, E. A.; Wormeester, H.; Poelsema, B. *Langmuir*, **18**, 7677-7682, 2002.
b) Porter, L. A.; Choi, H. C.; Ribbe, A. E.; Buriak, J. M. *Nano Lett.*, **2**, 1067-1071, 2002.
c) Meltzer, S.; Resch, R.; Koel, B. E.; Thompson, M. E.; Madhukar, A.; Requicha, A.; Will, P. *Langmuir*, **17**, 1713-1718, 2001.
d) Brust, M.; Stuhr-Hansen, N.; Norgaard, K.; Christensen, J. B.; Nielsen, L. K.; Bjornholm, T. *Nano Lett.*, **1**, 189-191, 2001.
e) Harnisch, J. A.; Pris, A. D.; Porter, M. D. *J. Am. Chem. Soc.*, **123**, 5829-5830, 2001.
f) Jiang, P.; Xie, S.; Yao, J.; Gao, H.; Zhang, H.; Shi, D.; He, S.; Pang, S. *J. Chinese Electron Micr. Soc.*, **20**, 589-593, 2001.
g) Huang, S.; Tsutsui, G.; Sakaue, H.; Shinubara, S.; Takahagi, T. *J. Vac. Sci. Technol. B*, **18**, 2653-2657, 2000.
h) Li, W.; Huo, L.; Wang, D.; Zeng, G.; Xi, S.; Zhao, B.; Zhu, J.; Wang, J.; Shen, Y.; Lu, Z. *Colloids and Surfaces A: Physicochem. Eng. Aspects*, **175**, 217-223, 2000.
i) Musick, M. D.; Keating, C. D.; Lyon, L. A.; Botsko, S. L.; Pena, D. J.; Holliway, W. D.; McEvoy, T. M.; Richardson, J. N.; Natan, M. J. *Chem. Mater.*, **12**, 2869-2881, 2000.
j) Lee, I.; Chan, K.; Phillips, D. *Ultramicroscopy*, **75**, 69-76, 1998.
k) Grabar, K. C.; Brown, K. R.; Keating, C. D.; Stranick, S. J.; Tang, S.; Natan, M. J. *Anal. Chem.*, **69**, 471-477, 1997.
l) Schmid, G.; Peschel, St.; Sawitowski, Th. *Z. Anorg. All. Chem.*, **623**, 719-723, 1997.
m) Arcoleo, V.; Liveri, V. *Chem. Phys. Lett.*, **258**, 223-227, 1996.
n) Ramachandran, T. R.; Madhukar, A.; Chen, P.; Koel, B. E. *J. Vac. Sci. Technol. A*, **16**, 1425-1429, 1998.
o) Luo, J.; Jones, V. W.; Maye, M. M.; Han, L.; Kariuki, N. N.; Zhong, C. *J. Am. Chem. Soc.*, ASAP, 2003.

8. a) Li, Q.; Zheng, J.; Liu, Z. *Langmuir*, **19**, 166-171, 2003.
b) Porter, L.; Choi, H. C.; Schmeltzer, J. M.; Ribbe, A. E.; Elliot, L; Buriak, J. M. *Nano Lett.*, **2**, 1369-1372, 2002.
c) Garno, J. C.; Yang, Y.; Amro, N. A.; Cruchon-Dupeyrat, S.; Chen, S.; Liu, G. *Nano Lett.*, **3**, 389-395, 2003.
d) Han, S.; Shi, X.; Zhou, F. *Nano Lett.*, **2**, 97-100, 2002.
e) Liu, S.; Maoz, R.; Schmid, G.; Sagiv, J. *Nano Lett.*, **2**, 1055-1060, 2002.
f) Zheng, J.; Chen, Z.; Liu, Z. *Langmuir*, **16**, 9673-9676, 2000.
g) He, H. X.; Zhang, H.; Li, Q.C.; Zhu, T.; Li, S.; Liu, Z. F. *Langmuir*, **16**, 3846-3851, 2000.

9. Kim, D.I., Islam, M.A., Avila, L., Herman I.P. *J. Phys.Chem.* B, **107**, 6318, 2003.

10. Prasad, B. L. V.; Stoeva, S. I.; Sorensen, C.M.; Klabunde, K. J. *Langmuir*, **18**, 7515-7520, 2002.

11. Prasad, B. L. V.; Stoeva, S. I.; Sorensen, C.M.; Klabunde, K. J. *Chem. Mater.*, **15**, 935-942, 2003.

12. Stoeva, S. I.; Prasad, B. L.V.; Sitharaman, U.; Stoimenov, P. K.; Zaikovski, V.; Sorensen, C. M.; Klabunde, K. J. *J. Phys. Chem. B*, **107**, 7441-7448, 2003.

13. Kralchevsky, P. A.; Nagayama, K. *Particles at Fluids Interfaces and Membranes*, Elsevier, 517-590 and references in Chapter 13, 2001.

14. a) Ramirez-Aguilar K. A.; Rowlen, K. L. *Langmuir*, **14**, 2562-2566, 1998.
b) Hsieh, S.; Meltzer, S.; Wang, C. R.; Requicha, A.; Thompson, M. E.; Koel, B. E. *J. Phys. Chem. B*, **106**, 231-234, 2002.
c) Ebenstein, Y.; Nahum, E.; Banin, U. *Nano Lett.*, **123**, 5829-5830, 2002.
d) Nath, N.; Chikoti, A. *Anal. Chem.*, **74**, 504-509, 2002.
e) Grabar, K. C.; Allison, K. J.; Baker, B. E.; Bright, R. M.; Brown, K. R.; Freeman, G.; Fox, A. P.; Keating, C. D.; Musick, M. D.; Natan, M. J. *Langmuir*, **12**, 2353-2361, 1996.

15. Maeda, H.; Maeda, Y. *Nano Lett.*, **2**, 1073-1077, 2002.

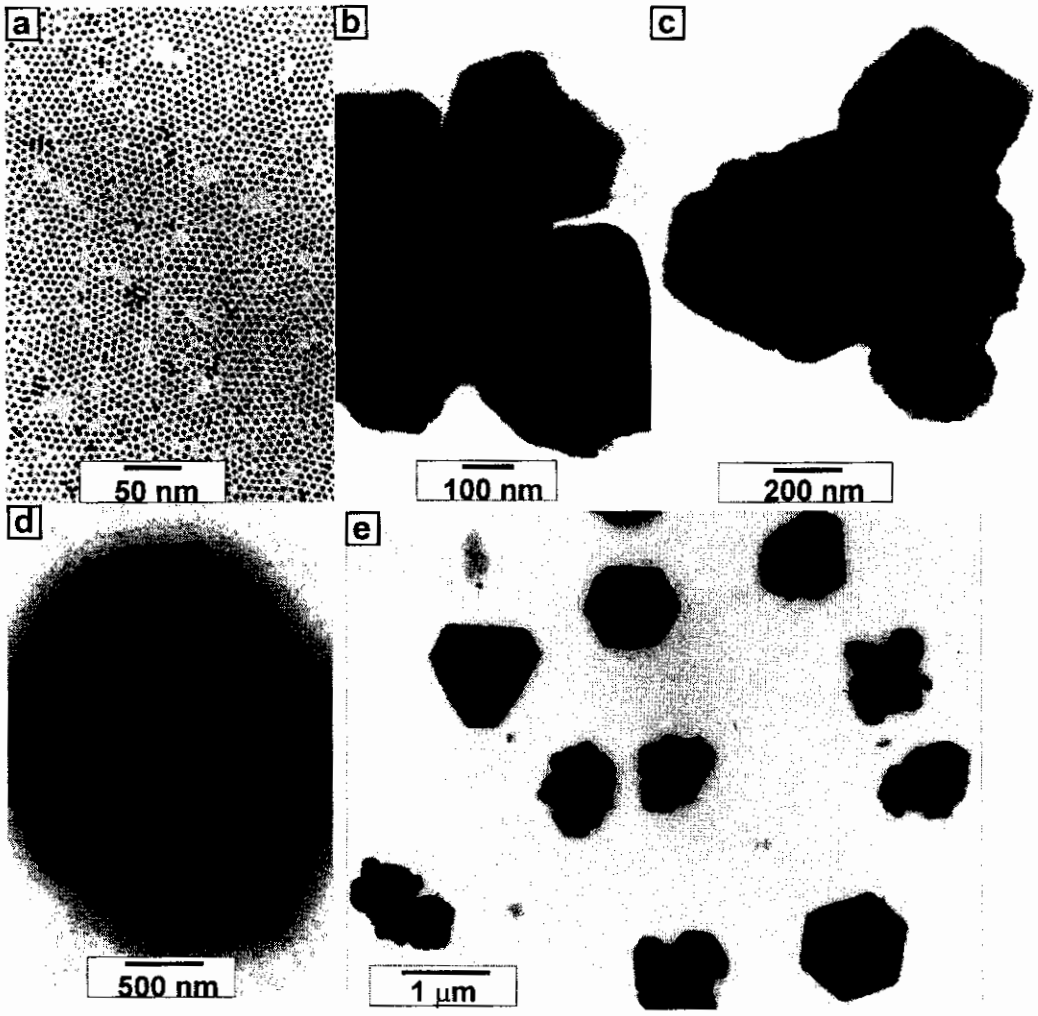

Figure 1 – a) Representative Au nanoparticles with 4.7 nm average diameter stabilized by $C_{10}H_{21}SH$ and $C_{12}H_{25}SH$ imaged by TEM; b) TEM of NCSs formed by $C_{10}H_{21}SH$ – functionalized nanoparticles; c), d), and e) TEM of NCSs in case of $C_{12}H_{25}SH$ – stabilized particles.

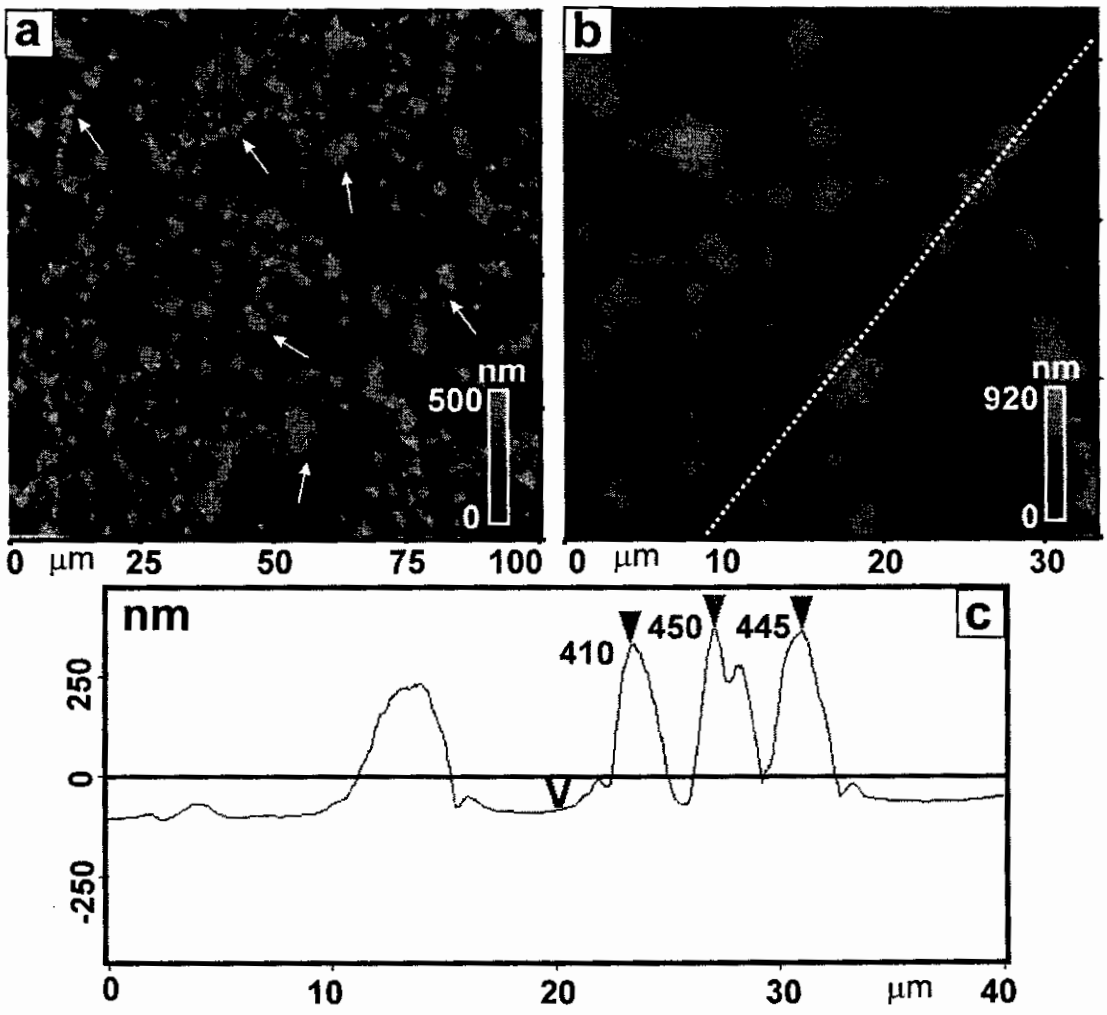

Figure 2 – a) and b) TM-AFM images of $C_{10}H_{21}SH$-stabilized Au NCSs formed on hydrophobic supports; c) cross-section along the line shown in b).

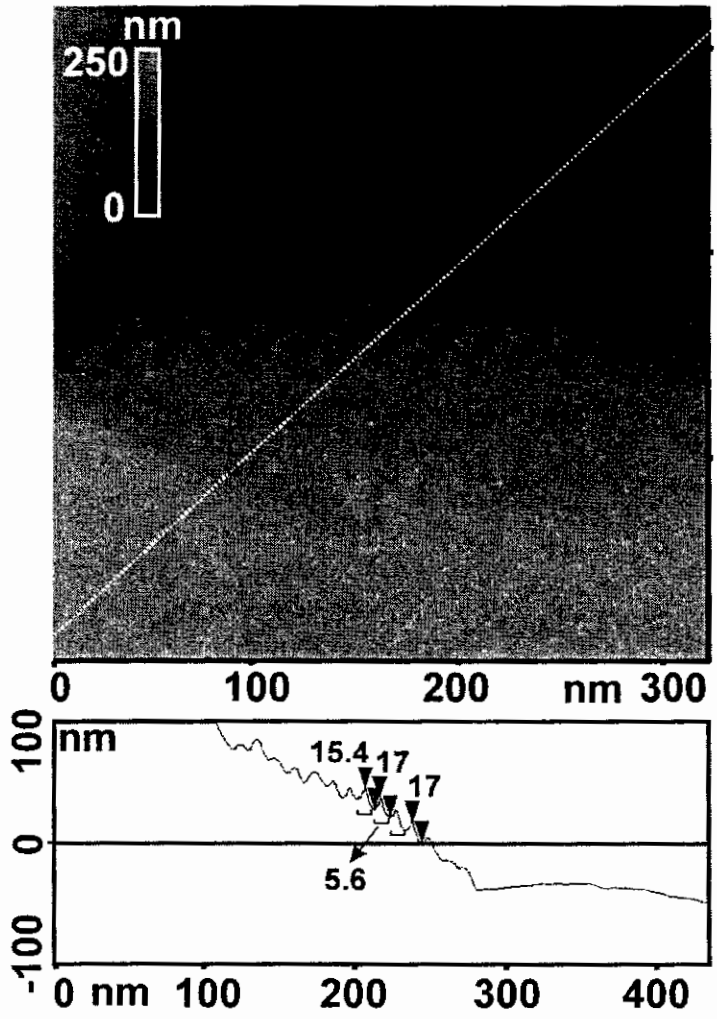

Figure 3 – TM-AFM of a resolved superlattice edge in case of $C_{10}H_{21}SH$-stabilized Au nanoparticles on hydrophobic support and the corresponding cross-section along the line in the AFM image. (Note the 'terraced-like' arrangement of the particles.)

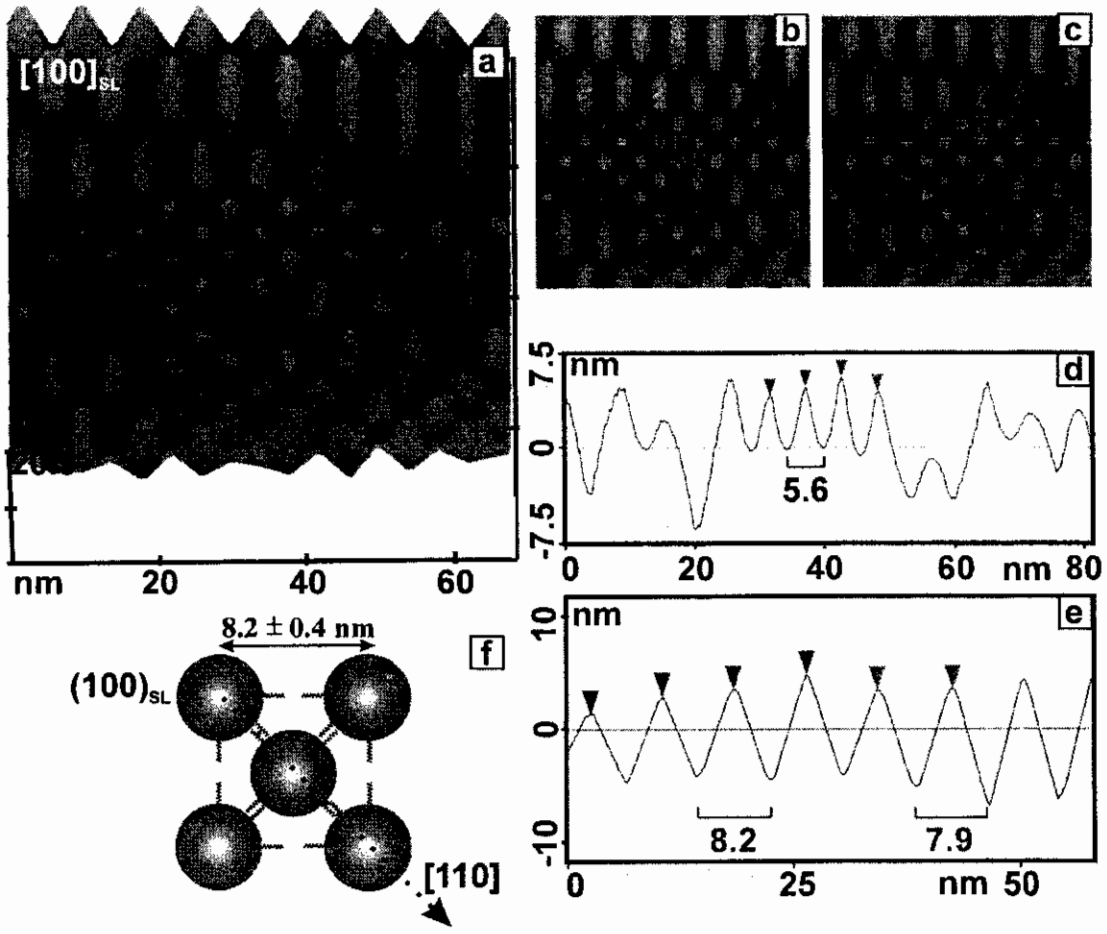

Figure 4 – a) 3D TM-AFM image of (100) surface of *fcc* NCS formed by $C_{12}H_{25}SH$-stabilized Au nanoparticles on carbon-coated glass support; b) and c) 2D TM-AFM of a); d) Cross-section along the line in b); e) Cross-section along the line in c); f) Schematic representation of (100)SL surface of *fcc* NCS together with the stabilizing thiol molecules.

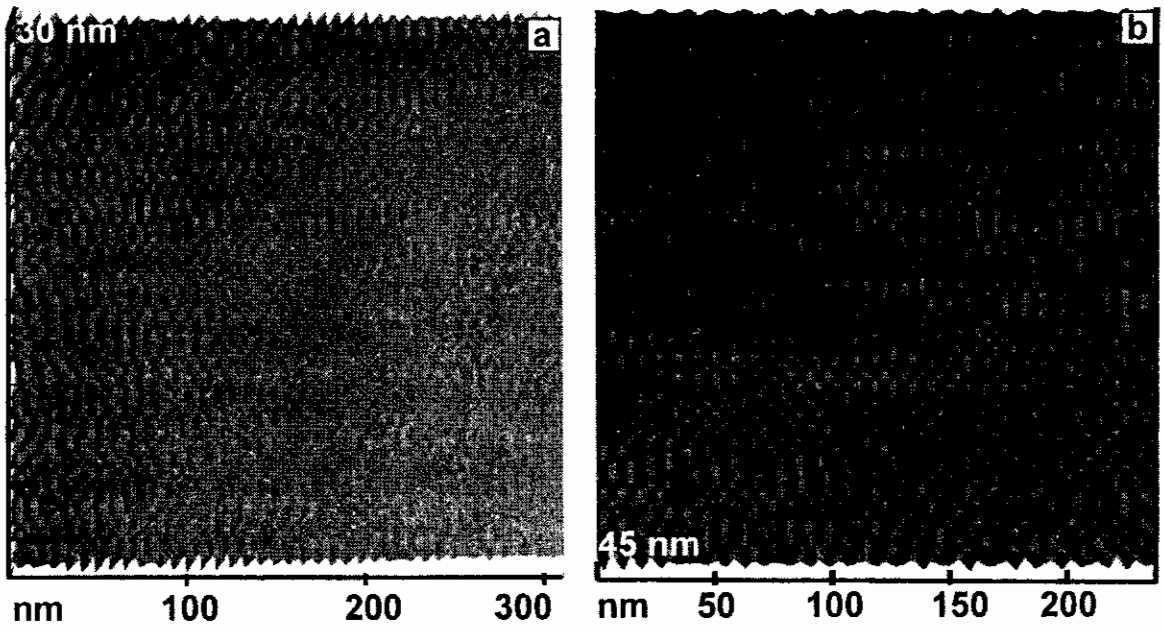

Figure 5 – a) and b) 3D TM-AFM image of NCSs formed by $C_{12}H_{25}SH$-satbilized Au nanoparticles on hydrophobic glass support. The particle size and interparticle spacing are the same as those in Figure 4.